December, 2007

A bubble-powered micro-rotor: conception, manufacturing, assembly and characterization

Jonathan Kao
Xiaolin Wang
John Warren, *Brookhaven National Laboratory*
Jie Xu, *Columbia University*
Daniel Attinger, *Columbia University*

A bubble-powered micro-rotor: conception, manufacturing, assembly, and characterization

Jonathan Kao*, Xiaolin Wang*, John Warren, Jie Xu# and Daniel Attinger#**

** State University of New York at Stony Brook, Stony Brook NY 11794*

***Brookhaven National Laboratory, Upton NY 11973*

#Columbia University, New York NY 10027

E-mail: da2203@columbia.edu (Daniel Attinger)

Abstract

A steady fluid flow, called microstreaming, can be generated in the vicinity of a micro-bubble excited by ultrasound. In this article, we use this phenomenon to assemble and power a microfabricated rotor at rotation speeds as high as 625 rpm. The extractible power is estimated to be on the order of a few femtowatts. A first series of experiments with uncontrolled rotor shapes is presented, demonstrating the possibility of this novel actuation scheme. A second series of experiments with 65 μm rotors micromanufactured in SU-8 resin is then presented. Variables controlling the rotation speed and rotor stability are investigated, such as the bubble diameter, the acoustic excitation frequency and amplitude, and the rotor geometry. Finally, an outlook is provided on developing this micro-rotor into a MEMS-based motor capable of delivering tunable, infinitesimal rotary power at the microscale.

1. Introduction

Since the 1990's, there have been significant research efforts devoted to the development of micro-motors and actuators. These devices are for instance needed for novel power supply schemes for microelectronic devices [1-3], for biomedical applications where micro-motors [4] drive drug delivery systems, surgical tools, probes, and for biomechanical actuators for biological cells [5]. Two approaches can be used to achieve these ends. A first approach is to

This is a manuscript from *Journal of Micromechanics and Microengineering* 17 (2007): 2454, doi:10.1088/0960-1317/17/12/010.
Posted with permission.

miniaturize an existing macroscopic concept. With photolithography, micro gas turbines [1-3], a miniature Wankel engine [6], and electrostatic micro-motors [4] have been created. These prototypes are remarkable due to their complexity and high power density, on the order of 100MW/m^3. Miniaturization, however, presents inherent difficulties because the ratio of surface forces to volume forces is inversely proportional to the device size. Therefore, friction, wear, and geometric tolerance issues become challenging at the microscale. The second approach to develop micro-motors and actuators takes advantage of the increasing importance of surface forces inherent to the miniaturization process. This way, designs of greater simplicity can be produced, exemplified by the bubble-jet printing technology, where an explosive bubble acts as a piston [7], or a recently demonstrated linear propulsion system driven by a bubble oscillating in a channel [8]. It must be stated that these simpler designs sometimes go along with complex thermofluidic phenomena [9], because of the strong coupling of transport phenomena, and the very small time and space scales involved. The novel rotor actuation concept that we present also takes advantage of this second approach, using the micro-flow in the vicinity of a sonicated micro-bubble to assemble a micro-rotor on top of a microbubble and induce a steady rotation of the rotor.

The working principle of the micro-rotor presented here can be described as follows. When a gas bubble in a liquid is excited by ultrasound, it oscillates according to the Rayleigh-Plesset equation [10]. For a free-floating bubble, the surrounding liquid participates to these oscillations with a symmetrical, radial motion. In the case where the oscillating bubble is attached to a solid wall, as in the case relevant to this article, the motion of the surrounding liquid is not radially-symmetrical anymore and the bubble-liquid interface exhibits a coupling of radial and translational motion, through respective expansion (or contraction) and translation perpendicular to the wall. This specific liquid motion involves a first order, high-frequency, oscillatory flow, as well as a second-order, low-frequency, steady vortical flow. This latter flow, called acoustic streaming, has been expressed by Longuet-Higgins [11] for a bubble in bulk liquid with a viscous stream function ψ_1 involving a finite number of Stokes singularities as $\psi_1 = \psi_0 / 2 \left(-8r/d + d/r + (d/r)^4\right)\sin^2\theta$. In the above equation, d is the bubble diameter, r is the distance to the bubble center, θ is the angle with the axis of translation of the bubble, and the

base stream function ψ_0 is function of the bubble size, the phase shift between the radial and translational oscillations of the bubble, and the oscillation frequency and amplitude. The velocities are easily derived from the stream function [11, 12]. The presence of a wall attached to the bubble can be handled by adding a system of mirror singularities to the above stream function [13], and the full derivation of the stream function for that particular case is presented in [14]. Qualitatively, the steady flow resulting from the sonication of a microbubble attached to a wall corresponds to a vortical flow structure that is radially symmetric with respect to the normal vector to the surface where the bubble is attached. In simpler words, the streamlines have the donut-shaped pattern shown in Figure 1a. The analytical solution shown in Figure 1a agrees reasonably well with flow visualization using particles as tracers [14], both in terms of flow structure and velocities, with a maximum velocity magnitude on the order of 1 mm/s. This acoustic streaming flow, also called microstreaming, was recently investigated theoretically [11] and exploited to control the deformation and rupture of biological vesicles [13]. As demonstrated by the experiments below, this microstreaming flow can also be exploited to assemble a micro-rotor on the surface of a bubble and control its rotation speed. This novel process works with two kinds of rotors: rotors with uncontrolled shapes (section 2) and rotors with controlled, micromanufactured shapes (section 3 and 4).

Comment [F1]: Daniel: Only reference 7 has the definition of the stream fuction as we use it, although 12 does give a theretical eplanation for the use of stream fnctions

2. Feasibility of a bubble-powered micro-rotor

This section describes the experimental setup and a first series of experiments that demonstrate the feasibility of actuating a micro-rotor by a sonicated bubble.

2.1. Experimental setup

The experimental setup is shown in Figure 2. Experiments take place in a 10 mL glass cuvette with a piezoelectric ceramic transducer (PZT) glued to its bottom. The transducer allows for the generation and control of a standing pressure wave in the fluid contained in the cuvette. In the cuvette, a resistance microheater (Heraeus, Germany) generates isolated micro-bubbles on its surface by gas desorption from the gently heated liquid. The fluid temperature increase ΔT due to the microheater use can be estimated by equating the enthalpy change of the liquid in the

cuvette with the electrical power given to the resistor. This gives $\rho V c_p \Delta T = UI$, with V = 10 mL, U = 5 V and I = 0.5 A. Using the physical properties of water and a typical heating time of 5 s, an average temperature increase of 0.3 K is calculated, which is negligible.

A 15 MHz waveform generator connected to a 500kHz amplifier (Krohn-Hite 7600 M, 200 V) provides an AC voltage V_{trans} to the piezoelectric transducer. A high-speed camera (Pixelink PL-A741) coupled to a Mitutoyo 70XL microscope zoom is used to observe the motion of the rotor, with temporal and spatial resolutions on the respective order of one μs and one μm and frame rates ranging from 20 to 330 fps. A delay generator is used to pulse a diode to image the oscillations of the bubble driven by the standing pressure wave.

2.2. Preliminary experimentation with polymer spheres and debris

In order to visualize the flow, polymer spheres were mixed with water in the cuvette chamber. Using acoustic waves at 180 kHz and bubbles about 40 μm in diameter attached to the surface of the much larger resistance heater, steady microstreaming flows were observed in the vicinity of the sonicated bubbles. The flow pattern was found to correspond to the analytical flow pattern shown in Figure 1a.

Flow visualization experiments were performed with polymer spheres (Eichrom Technologies Inc., Pre-Filter Resin) introduced in water to mimic more precise Particle-Image-Velocimetry (PIV) methods [15]. The 110-150 micrometer particles were crushed in order to obtain smaller particles that would better follow the flow. The general flow pattern was found to agree quantitatively and qualitatively [14] with the simulation in Figure 1a. Remarkably, we found that larger polymer debris [14] such as the slightly asymmetric spherical cap depicted in Figure 3, were attracted to the surface of the bubble upon which they would begin to rotate, in the configuration shown in Figure 3, where the wall is vertical at the left of the bubble. This process was repeated with debris of various shapes and sizes comparable to the bubble, and occurred according to the three following steps: (1) a debris caught in the vortical microstreaming flow moves towards the bubble along one of the streamlines depicted in Figure 1, (2) the debris self-centers on the surface of the bubble, and (3) the debris starts rotating around the bubble's axis of symmetry, most likely due to the symmetrical nature of the microstreaming flow. These three steps describe a self-assembly and actuation process that takes approximately 1 second. The rotor pictured in Figure 3 rotated at a speed of 300 rpm [14]. Also, experiments

Comment [IK2]: Hi Professor, in section (2.2), I'm not sure if PIV methods not sure if methods is supposed to be plural or singular. If singular, then delete s on methods and reinsert a.

Comment [IK3]: In section 2.2, not sure if you want to keep this, but I just put in "upon which they would begin to rotate" to try to make clear that the debris rotates on the bubble. If you think this is assumed or doesn't work as well, it's fine to remove.

in [14] showed that the rotor frequency could be controlled by varying the acoustic frequency. This first series of experiments showed the possibility of actuating a micro-rotor by acoustic waves, but did not allow any control or measurement of the rotor geometry.

3. Manufacturing micro-rotors with controlled geometries

A second series of experiments were performed with micro-manufactured rotors. Three types of micro-rotors were designed with diameters of 65 μm and geometries as shown in Figure 4. The rotor geometries are bio-inspired, mimicking the general shape of the winged seed (samara) of a Stony Brook maple tree. One type is a single layer rotor (A1) while the other two types (A2 and B2) have two layers to better imitate the vein visible on the winged seed. Three batches of micro-rotors were fabricated using optical lithography to pattern SU-8, an epoxy-based photoresist used to fabricate high aspect ratio microstructures for MEMS applications. Due to the delicate optical alignment of the second mask with respect to the first, there is significant misalignment between the two layers in A2-type rotors, while B2-type rotors have only a slight misalignment. A Dektak profilometer measured the thickness of A1-type rotors to be 1.87 μm while B2-type rotors have a thickness of 1.98 μm for the layer in contact with the bubble (Figure 1b) and a second layer thickness of 2.20 μm. Thousands of micro-rotors were patterned on separate silicon wafers covered with a 17 nm release layer (XP-SU8, Microchem Corp). The rotors were released by submerging the wafers in an ammonium hydroxide solution and using a water mini-jet. The solution with the floating rotors was then neutralized with sulfuric acid to pH 7. A Brookfield viscometer measures the solution viscosity to be 1.1 $\pm$ 0.1 cP, a value close to the viscosity of water.

4. Actuation and characterization of the micro-fabricated micro-rotors

This section describes the actuation process of the micro-rotors and characterizes the parameters affecting rotation speed and stability.

4.1. Micro-rotors assembly and actuation

The assembly and actuation of the micro-rotors was done using the procedure detailed in section 2.2, which involves the successive steps: a micro-bubble is generated on the surface of a millimeter-size heater, ultrasound creates a microstreaming flow that attracts one drifting rotor

towards the bubble, the rotor self-centers on top of the bubble, in the configuration of Figure 1c, and starts rotating. Since thousands of rotors were drifting in the cuvette, the assembly could be made in a relatively quick and reproducible manner. The observed direction of the rotation is shown by arrows in Figure 4. Using an appropriate intensity and frequency of ultrasound, a rotor would rotate for several minutes on top of the bubble.

4.2. Characterization

Using video microscopy, we observed the trajectories of the rotors in the cuvette: they would drift slowly in a linear motion, both in the presence or absence of ultrasound. However, once the ultrasonic excitation would induce the self-assembly of a rotor on top of a sonicated bubble, the rotor would start to rotate in a plane parallel to the wall where the bubble was sitting. We verified that the rotation was caused by the conjunction of the ultrasound and the bubble-rotor coupling by stopping the acoustic excitation: the rotor would immediately disassemble from the bubble and start drifting away without visible rotation.

The rotation angle α and the rotation speed n were measured by visual inspection of high-speed videos of the rotating rotor. A typical frame rate was 328 frames per second, and the relative error in rotation speed was estimated as +/- the inverse of the number of frames observed for one full revolution. Our characterization study identified that the rotation speed n depends on the following parameters: the angle α between the rotor plane and the solid surface where the bubble sits; the bubble diameter d; the driving ultrasonic frequency f; the voltage applied to the piezoelectric transducer V_{trans}; and the type of micro-rotor geometry (A1, A2, or B2 as shown in Figure 4). The uncertainty on the bubble diameter was estimated to be +/- 2 pixels in the image plane, corresponding to +/- 1 micrometer. The largest rotation frequencies and most stable experiments were obtained with ultrasound excitation frequencies corresponding to the natural frequency of the cuvette (161.6 kHz) and with bubbles with diameters close to 40 micrometer.

4.2.1. Influence of ultrasonic excitation frequency

The frequency response of the micro-rotors was assessed by varying the frequency of the acoustic excitation in the vicinity of the frequency maximizing the rotation speed. Figure 5 depicts the respective frequency response of type B2 micro-rotors. Similar curve shapes were obtained for the other two types of rotors (A1 and B1), although with lower maximum rotation

speeds. Clearly, the rotation speed is maximized when the excitation frequency matches the resonant frequency of the bubble-cuvette system. The frequency response curve is analogous to the frequency response of linear spring-inertia-dashpot system [16], where the response is relatively constant for under-critical excitation frequencies, peaks at the natural frequency, and vanishes for over-critical excitation frequencies. In the system described here, the surface tension is the spring, and the inertia and dashpot correspond to the complex motion of the fluid and its interaction with the propeller. In the case of the micro-rotor, over-critical excitation frequencies would sometimes correspond to cases where the rotor stops turning. Obviously, the rotation speed is very sensitive to the excitation frequency. This high sensitivity is interesting since excitation frequency is a parameter that is easy to control with a high precision.

4.2.2. Influence of the bubble diameter

Our experiments in Figure 6 describe the relation between the rotor rotation speed and the bubble equivalent diameter $\bar{d}$ (the diameter of a spherical bubble with a similar volume as the spherical cap volume). Five sets of data are plotted, with the excitation frequency and voltage being kept constant within each set. The data in Figure 6 shows a peak in micro-rotor rotation speed for a bubble diameter of 36 micrometer, with rotation speeds decreasing with increasing bubble diameter.

This behavior can be explained by considering that the bubble diameter d and bubble natural frequency f_b are related by the relation $d f_b = 6\ m/s$[10]. This relation predicts that a bubble with a resonance frequency that matches the cuvette resonant frequency of 161.6 kHz has a diameter of 38 μm. It is therefore a reasonable guess to assume that exciting a bubble at its resonance frequency would maximize the associated microstreaming and the rotation speed of the rotor. It is worth mentioning that we were not able to perform experiments with bubbles smaller than this optimal diameter, except at the lowest excitation voltage of 20V. This can be explained by the fact that the rate of interfacial diffusion of the bubble gas into the water increases with ultrasound level and bubble curvature [10], causing smaller bubbles to shrink and disappear within seconds.

4.2.3. Voltage applied to the piezoelectric transducer

In Figure 7, the rotation speed is plotted as a function of the voltage applied to the transducer, for a rotor of type A2. The rotation speed increases monotonically with the transducer voltage V_{trans},

which can be explained by the fact that the energy delivered to the system increases. A linear regression best fit of the experimental data for A2-geometry gives the following equation n=6.18V_{trans}–311 [rpm]. It must be mentioned that the streaming speed usually grows quadratically with the ultrasonic intensity, a behavior characteristic of the second-order streaming flow [11, 17]. Given the narrow range of voltages used in Figure 7, it is difficult to determine if the voltage-rotation speed relationship is linear or quadratic. The reason our measurements were performed only for a relatively narrow interval of voltages is that voltages higher than 80V would make the rotor wobble and leave the bubble. It must also be mentioned that more direct ways exist to measure the energy delivered to the system, such as a needle hydrophone, but this device was not available for our measurements.

4.2.4. Influence of rotor geometry

High-speed visualization and measurements were made with the three types of rotors to determine what rotor geometry (type A1, A2 and B2 as shown in Figure 4) would work best. The rotor geometry was found to influence the rotation in three ways: the regularity of the rotation, the rotation angle α between the rotor plane and the solid surface plane, and the rotation speed n. In most cases, a large value of α would correspond to unstable rotation and detachment of the rotor from the bubble. A1-type rotors were observed behaving erratically, e.g. making a revolution in one direction, and then revolving in the reverse direction, in addition to changing their contact point over the surface of the bubble. A2-type rotors typically rotate with α =15° to 30°, probably due to the misalignment between the two layers, but never span erratically. Finally, the best results were obtained with B2-type rotors: they rotate with α = 0° and with high regularity. Furthermore, the maximum rotation speeds observed for the A1, A2, and B2 rotors were 33 rpm, 300 rpm, and 625 rpm, respectively. These results confirm that geometry is a critical parameter for rotor stability and maximizing rotor rotational speeds. Furthermore, these results show that the double layer design, which more accurately mimics the winged seed shown in Figure 4, is more stable and rotates about 20 times faster than the single layer design. Also, our results suggest that misalignment between the two layers should be minimized for stability and efficiency purposes, as exemplified by the better stability and rotation speed of rotors B2 in comparison with rotors A2. To this end, it is evident that optimizing rotor geometry is critical to maximizing rotational speed and extractible power. This is however not a trivial task, because

the physics of the problem involves the complex coupling of high-frequency, transient ultrasound and free surface oscillations with a steady, second-order, highly viscous flow, as well as the interaction of this complex flow with a complex solid shape that is free to move.

4.3. Power output

The power output of these rotors can be estimated as follows. At low Reynolds numbers, the power given by the fluid to the rotor is approximately equal to the viscous dissipation that would be produced by the rotation of a similar rotor, at a similar speed, in a quiescent fluid. Von Karman solved the laminar flow created by a rotating disk, and the corresponding torque on one side of the disk is given in [18] as $M = 0.62\frac{\pi}{32}\rho d^4\sqrt{\upsilon\omega^3}$, where ρ is the density and ν is the kinematic viscosity of the surrounding fluid. The rotary power can therefore be estimated as $P = 2M\omega$. Using the physical properties of water, the diameter of the manufactured rotor, and a rotation speed of ω = 65/s (625 rpm), we obtain a power output on the order of P = 74 femtowatt. This is obviously a very low power, however it is obtained by a very simple, self-assembled microdevice and can be precisely tuned by e.g. tuning the excitation frequency. The efficiency of the rotor actuation can be estimated by the ratio of the power output of a single rotor and the power needed by the electric amplifier (Krohn Hite 7600M, 200W input power) that drives the piezoelectric actuator. Obviously, the efficiency of a motor built on this principle would be extremely small, however it is a common feature of micro-actuators. For instance the widely-used thermal ink-jet actuator has an efficiency on the order of $1x10^{-4}$ [19]. Our opinion is that the success of a micro-actuator is not primarily driven by energy efficiency, but rather by issues such as compactness, ease of manufacturing, ease of actuation and control, and adequacy to the task.

5. Outlook

A tentative design to extract rotary power from the rotor presented in this article is proposed in Figure 8. A sub-micrometer diameter shaft can be attached perpendicularly to the rotor to transmit the mechanical power through the bubble and the solid wall. Multiwall carbon nanotubes can be used to build the shaft, because they have a sub-micrometer diameter, can sustain a torque three orders of magnitude higher [20] than the one provided by the rotor, and exhibit extremely low relative friction. Therefore, an outer tube will be glued to the wall where

the bubbles will be generated, with e.g. patterned micro-heaters, while the inner tube will remain attached to the rotor. It is worth mentioning that a microbubble can easily form around a solid structure (the shaft in the present case) if the wetting properties of the solid structure are selected carefully. The eventuality that the bubble might 'pop out' because an object goes through it is only relevant to bubbles much larger than the one used in this study. Alternatively, biofibers can be used as a shaft. This system may also be scaled down, provided that the bubble is sufficiently stable to degassing [10], an issue which can be addressed with surfactants and the use of different gases and liquids. Furthermore, because only one dimension is required to control the frequency of a standing acoustic wave, concentric geometries can be used to minimize the total volume of the micromotor housing, as shown in Figure 8a. It is also possible to fit several motors in series in a space as thin as human hair, as pictured in Figure 8b. Finally, remote activation (through acoustic wave) allows design and activation of micro-motors in parallel, as well as selectivity between bubbles of different sizes. By conveniently controlling the excitation amplitude and frequency, the proposed micro-motor solutions will be capable of delivering infinitesimal torque at the microscale, with applications in micromixing and controlled excitation of biological structures with a rotary motion.

6. Conclusions

The feasibility of an acoustic, bubble-powered micro-rotor is demonstrated. A steady vortical microstreaming flow is used to self-assemble and actuate a micro-rotor on the surface of the bubble. Measurements with a high-speed camera have determined how the rotation speed and stability is affected by the bubble diameter, the excitation frequency and voltage, and the rotor geometry. Our measurements show that the frequency response of the rotor to the excitation frequency is analogous to the frequency response of a linear spring-inertia-dashpot system. High sensitivity to the excitation frequency provides a convenient way to control the rotation speed. Finally, designs are presented that will allow the use of this micro-rotor concept to apply controllable and infinitesimal torque at the microscale.

Acknowledgements

This research was supported by the NSF CAREER grant 0449269**.** This research was carried out in part at the Center for Functional Nanomaterials, Brookhaven National Laboratory, which is supported by the U.S. Department of Energy, Division of Materials Sciences and Division of Chemical Sciences, under Contract No. DE-AC02-98CH10886. Jonathan Kao was supported by the Simon's fellowship program at Stony Brook University. Daniel Attinger thanks Howard Stone, from Harvard University, for useful discussions on Stokes flows.

References

1. Peirs, J., D. Reynaerts, F. Verplaetsen, F. Norman, and S. Lefever. *Development of a micro gas turbine for electric power generation*. in *MME 2003, The 14th MicroMechanics Europe Workshop*. 2003.
2. Epstein, A.H. *Millimeter-scale, MEMS gas turbine engines*. in *Proceedings of ASME Turbo Expo 2003, Power for Land, Sea, and Air*. 2003.
3. Fréchette, L.G., S.A. Jacobson, K.S. Breuer, F.F. Ehrich, R. Ghodssi, R. Khanna, C.W. Wong, X. Zhang, M.A. Schmidt, and A.H. Epstein, *High-Speed Microfabricated Silicon Turbomachinery and Fluid Film Bearings.* J. Microelectromechanical Systems, 2005. **14**(1): p. 141-152.
4. Chapman, P.L. and P.T. Krein, *Smaller is Better? Perspective on Micro-motors and Electric Drives.* IEEE Industry Applications Magazine, 2003: p. 62-67.
5. Marmottant, P. and S. Hilgenfeldt, *A bubble-driven microfluidic transport element for bioengineering.* Proceedings National Academy of Sciences, 2004. **101**(26): p. 9523-9527.
6. Fu, K., A. Knobloch, F. Martinez, D.C. Walther, A.C. Fernandez-Pello, A.P. Pisano, and D. Liepmann, *Design and Fabrication of a Silicon-Based MEMS Rotary Engine*, in *Proc. ASME 2001 International Mechanical Engineering Congress and Exposition (IMECE), MEMS division*. 2001, ASME, New York: New York, NY.
7. Chen, P., W. Chen, P. Ding, and S. Chang, *Droplet formation of a thermal sideshooter inkjet printhead.* International Journal of heat and fluid flow, 1998. **19**(4): p. 382-390.
8. Dijkink, R., J. vanderDennen, C. Ohl, and A. Prosperetti, *The 'acoustic scallop': a bubble-powered actuator.* J. Micromech. Microeng., 2006. **16**(8): p. 1653-1659.
9. Glod, S., D. Poulikakos, Z. Zhao, and G. Yadigaroglu, *An Investigation of Microscale Explosive Vaporization of Water on an Ultrathin Pt Wire.* Int. J. Heat and Mass Transfer, 2002. **45**: p. 367-379.
10. Leighton, T.G., *The acoustic bubble*. 1994: Academic Press, London.
11. Longuet-Higgins, M.S., *Viscous streaming from an oscillating spherical bubble.* Proc. R. Soc. Lond. A, 1998. **454**: p. 725–742.
12. Pozrikidis, C., *Boundary Integral and Singularity Methods for Linearized Viscous Flow*. 1992: Cambridge Univ. Press, Cambridge, U.K.
13. Marmottant, P. and S. Hilgenfeldt, *Controlled vesicle deformation and lysis by single oscillating bubbles.* Nature, 2003. **423**: p. 153-156.
14. Wang, X., F. Moraga, and D. Attinger, *A micro-rotor driven by an acoustic bubble.* Nanoscale and Microscale Thermophysical Engineering, 2006. **10**(4): p. 379-385.
15. Meinhart, C.D., S.T. Wereley, and J.G. Santiago, *PIV measurements of a microchannel flow.* Experiments in Fluids, 1999. **27**: p. 414–419.
16. Meirovitch, L., *Fundamentals of Vibrations*. 2001: McGraw-Hill: New York, NY.
17. Xu, J. and D. Attinger, *Control and ultrasonic actuation of a gas-liquid interface in a microfluidic chip.* Journal for micromechanics and microengineering, 2007. **17**(609-616).
18. White, F., *Viscous Fluid Flow*. 3rd ed. 2006: McGraw Hill, section 3-8.2.
19. Nayve, R., M. Fujii, A. Fukugawa, T. Takeuchi, M. Murata, Y. Yamada, and M. Koyanagi, *High-Resolution Long-Array Thermal Ink Jet Printhead Fabricated by Anisotropic Wet Etching and Deep Si RIE.* Journal of Microelectromechanical Systems, 2004. **13**(5).

20. Ertekin, E. and D.C. Chrzan, *Ideal torsional strengths and stiffnesses of carbon nanotubes.* Physical Review B, 2005. **72**(4).

Figures

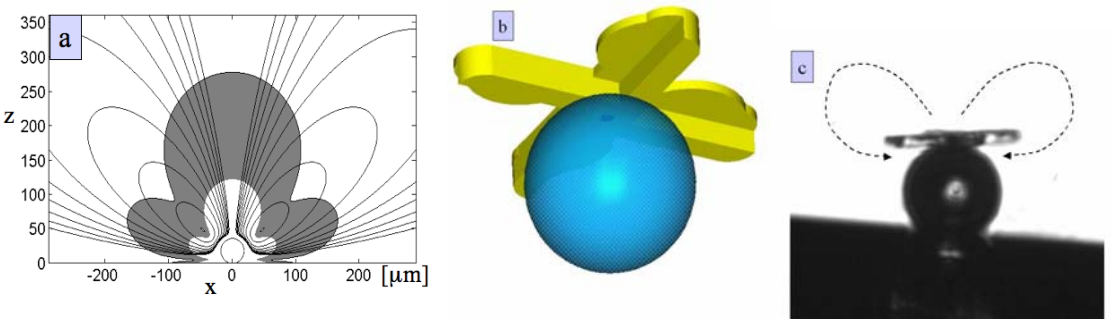

Figure 1: (a) Streamlines corresponding to the analytical solution of the microstreaming flow around a 36 µm diameter bubble [14]. The gray zone corresponds to velocities between 1mm/s (inner boundary of gray zone) and 0.1 mm/s (outer boundary of gray zone). (b) 3D model of the micro-rotor and the bubble (c) Photograph of the actual bubble-actuated micro-rotor. The microstreaming vortical flow streamlines are outlined by the dotted lines superimposed on the image. The rotor diameter is 65 µm. An *AVI* movie corresponding to figure 1c is available from stacks.iop.org/… **[EDITOR PLEASE FINALIZE]**

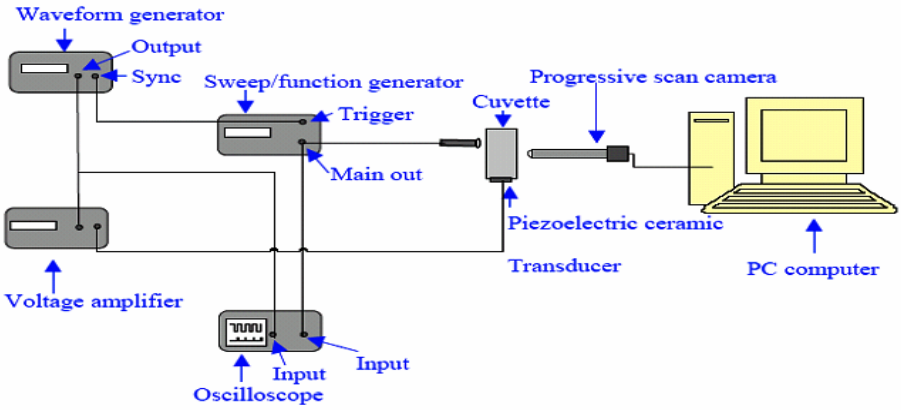

Figure 2: Experimental setup. The function and waveform generator are used to drive the illumination and piezoelectric excitation. The cuvette contains the micro-bubbles and the micro-rotors in solution.

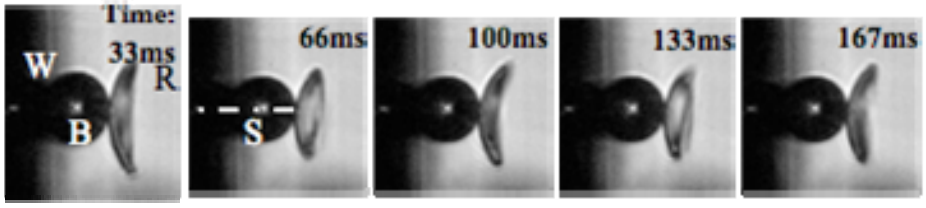

Figure 3: A slightly asymmetrical polymer rotor rotates at 300 rpm. The letters W, B, R, and S correspond respectively to the wall on which the bubble sits, the micro-bubble, the rotor, and the proposed shaft detailed in Section 5. An *AVI* movie corresponding to this case is available from stacks.iop.org/… **[EDITOR PLEASE FINALIZE]**

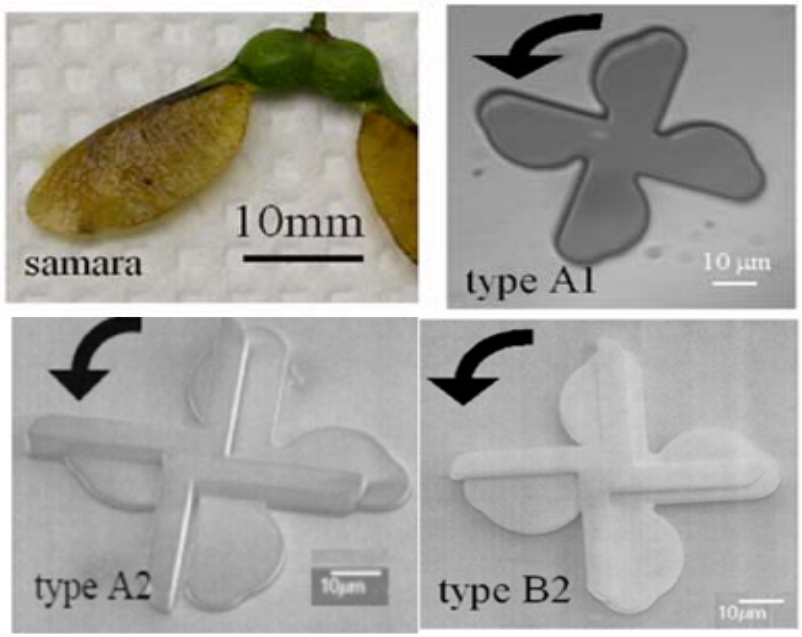

Figure 4: The geometry of the maple tree fruit or samara (top left), which inspired the rotor design. A1-type rotors are single layered. A2 and B2 rotors are double-layered; A2 has significant misalignment between the two layers, while B2 has less misalignment.

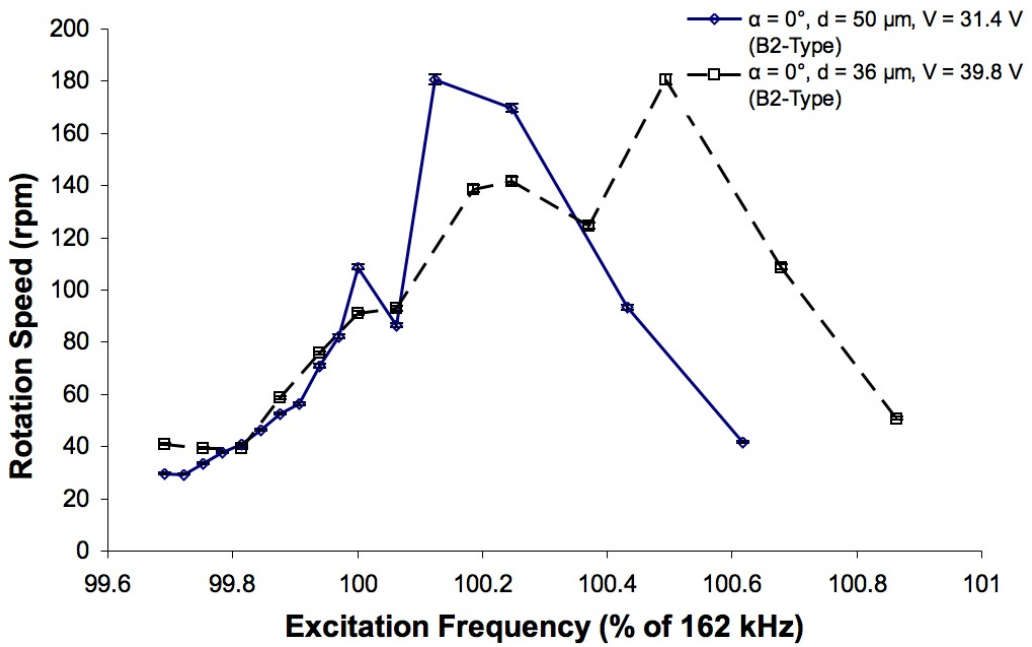

Figure 5: Influence of the excitation frequency on the rotational speed with B2-type rotors. The rotation speed is measured from high-speed visualization (328 fps). Errors on the rotation speed and frequency are minimal, because of the respective high frame rate and electronic frequency measurement.

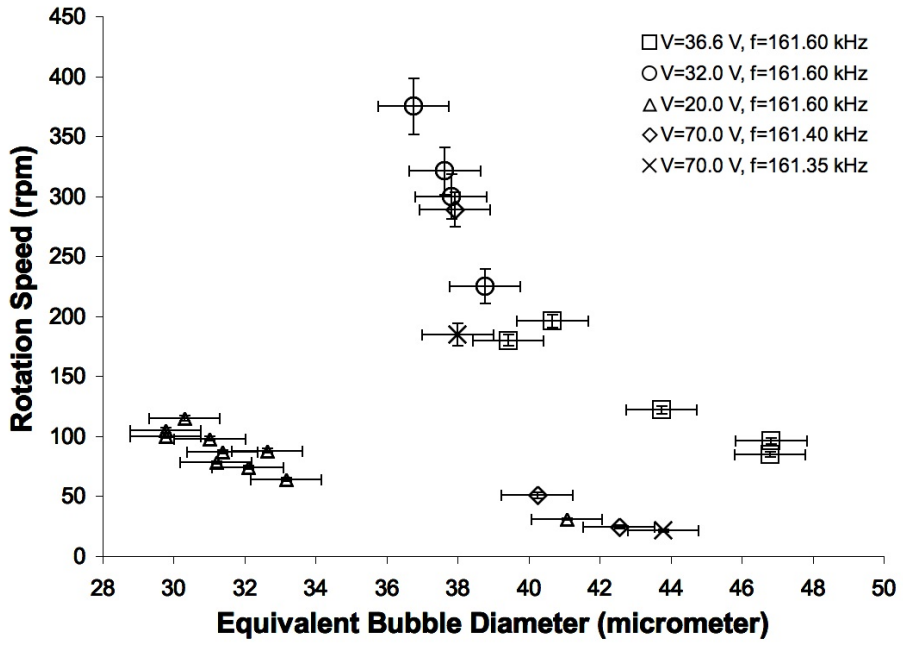

Figure 6: Measurements describing the effect of bubble equivalent diameter đ on rotation speed with B2-type rotors, for five sets of values of transducer voltage and excitation frequency. Error bars are calculated as in section 4.2.

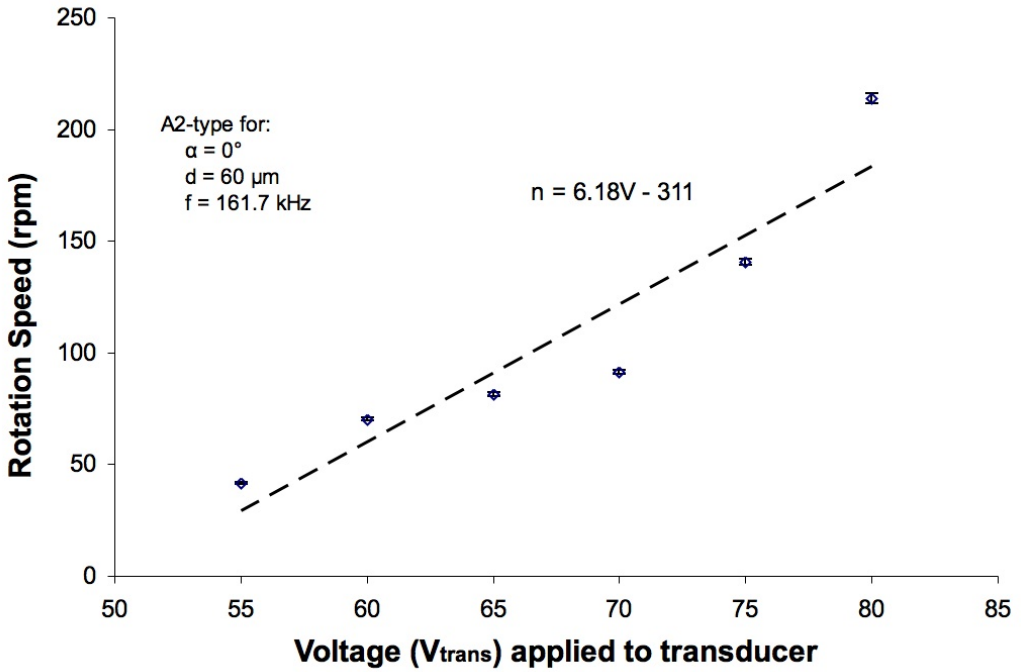

Figure 7: Rotation speed of a micro-rotor as a function of the voltage applied to the piezoelectric transducer. The rotation speed is measured from high-speed visualization (328 fps). Errors on the rotation speed and voltage are minimal, because of the respective high frame rate and electronic voltage measurement.

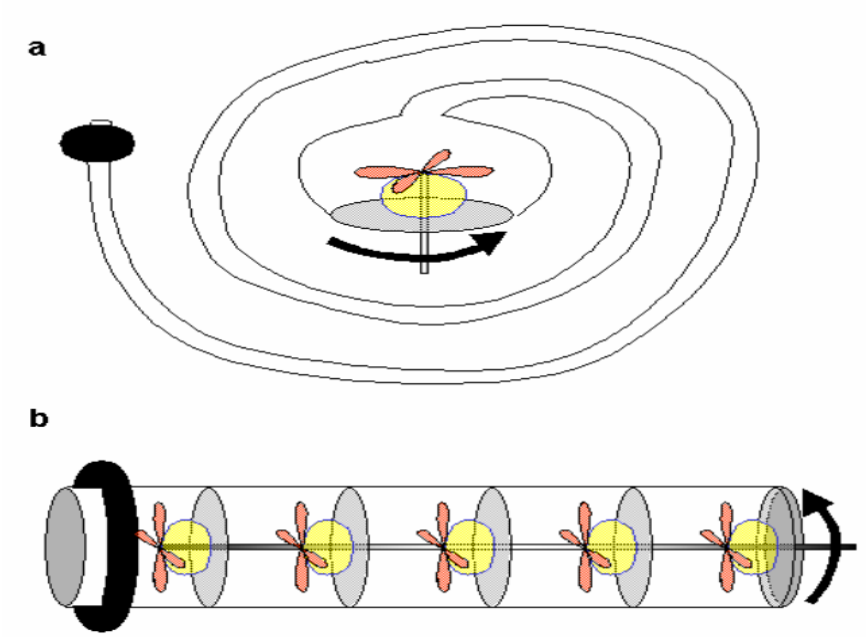

Figure 8: Tentative packaging of the micro-motor. The thick ring at the top is a piezoelectric transducer. In (a), a concentric geometry reduces the volume. In (b), five motors in series drive a unique shaft.